ISSN 1062-8738, Bulletin of the Russian Academy of Sciences. Physics, 2015, Vol. 79, No. 1, pp. 139–143. © Allerton Press, Inc., 2015.
Original Russian Text © A.A. Guda, I.A. Pankin, A.L. Bugaev, K.A. Lomachenko, S.A. Guda, V.P. Dmitriev, A.V. Soldatov, 2015, published in Izvestiya Rossiiskoi Akademii Nauk. Seriya Fizicheskaya, 2015, Vol. 79, No. 1, pp. 154–159.

X-ray Absorption Spectroscopy Determination of the Products of Manganese Borohydride Decomposition upon Heating

A. A. Guda[a], I. A. Pankin[a], A. L. Bugaev[a], K. A. Lomachenko[a], S. A. Guda[a], V. P. Dmitriev[a, b], and A. V. Soldatov[a]

[a]*Southern Federal University, Rostov-on-Don, 344090 Russia*
[b]*SNBL at ESRF, Polygone Scientifique Louis Néel, 38000 Grenoble, France*
e-mail: guda@sfedu.ru

Abstract—Manganese borohydride $Mn(BH_4)_2$ powder is heated in a hydrogen atmosphere in vacuum. The long-range order in the structure is monitored in situ by means of X-ray absorption spectroscopy and X-ray diffraction; short-range order, via Mg *K*-edge X-ray absorption near-edge structure spectroscopy. Above 120°C, the X-ray diffraction pattern disappears and an irreversible phase transition occurs, accompanied by sample amorphization and profuse hydrogen desorption. In the hydrogen atmosphere, the phase transition occurs at a temperature of ~110°C. The standard scheme of borohydride decomposition suggests hydrogen desorption and the formation of metallic manganese and boron. However, a theoretical analysis of X-ray absorption spectra shows that the most likely products of $Mn(BH_4)_2$ decomposition are manganese borides.

DOI: 10.3103/S1062873815010153

INTRODUCTION

Solid-state materials for hydrogen storage, e.g., metal borohydrides, are of great interest to researchers [1]. The most efficient hydrogen absorbers are alkali metal borohydrides; however, high temperatures of desorption (above 400°C for $LiBH_4$ [2, 3]) and limited numbers of working cycles complicate their use [4]. An alternative is transition metal compounds, particularly magnesium borohydride $Mg(BH_4)_2$ and isostructural manganese borohydride $Mn(BH_4)_2$, for which (according to data from thermogravimetric testing) hydrogen desorption exceeds 8 mass % in the temperature range of 100–200°C [5, 6]. The structures of these compounds [7] are trigonal crystal systems (sp. gr. $P3_112$) and are similar in porosity to metalorganic frameworks (MOFs). The $Mg(BH_4)_2$ structure contains pores that can absorb not only hydrogen and nitrogen but also small molecules like dichloromethane CH_2Cl_2 [8]. In addition, X-ray spectroscopy data indicate an intermediate amorphous phase in the pressure range 0.5–2 GPa. The amorphous phase then transforms into two mutually penetrating frameworks. Amorphization of the $Mg(BH_4)_2$ γ phase upon variation in pressure is another similarity between this material and MOFs and zeolites, in which a rigid porous structure collapses under pressure or upon heating and transforms into an amorphous solid.

The similarities between manganese $Mn(BH_4)_2$ and magnesium $Mg(BH_4)_2$ borohydride structures were also noted in [9], which was devoted to spectroscopic investigations of manganese borohydride $Mn(BH_4)_2$. The similarities were established through a comparative analysis of Raman and IR spectra. When manganese borohydride $Mn(BH_4)_2$ is heated, hydrogen is desorbed and the system loses its long-range order. The local structure of the reaction products can only be investigated using such localized techniques as X-ray absorption spectroscopy. The Raman and Fourier transform IR spectroscopy analysis of the final products of decomposition in [10] revealed the formation of amorphous boron and virtually no peaks corresponding to Mn–B oscillations.

In a manganese borohydride sample heated to 200°C, bonds are observed that can be attributed to oscillations in the Mn_3O_4 compound at 943 and 1039 cm^{-1} and oscillations corresponding to the amorphous B–B boron phase at frequencies of 1245 and 1331 cm^{-1}. In [10], in-situ measurements of X-ray diffraction (XRD) spectra were made. However, the obtained diffraction patterns contained no peaks of the metallic manganese phase. It is possible that Mn was contained in the reaction products in the form of either nanoparticles or an amorphous phase. An alternative version was the possible formation of amorphous manganese borides; however, neither Raman nor IR spectra showed any traces of Mn–B oscillations [10], due likely to the sample coming into contact with oxygen and the formation of oxides.

In this work, we investigate the local atomic structure of manganese in borohydride at different heating temperatures. Each sample was placed in an air-tight capillary filled with hydrogen or evacuated to a residual pressure of less than 1 mbar. Combining XRD and

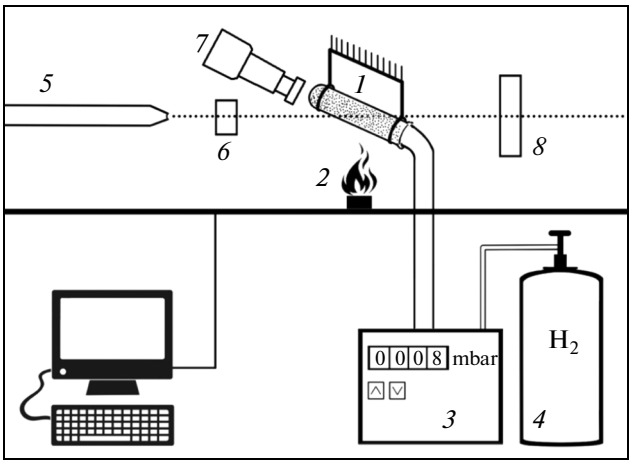

Fig. 1. Schematic of the experimental setup for simultaneous detection of X-ray diffraction and absorption spectra. Denotations are explained in the text.

X-ray absorption spectroscopy allows us to draw conclusions on the scheme of sample product decomposition, which is important for future use of the substance as a solid material for hydrogen storage.

EXPERIMENTAL

Our experiments were conducted on the BM01b Swiss–Norwegian experimental station at the European Synchrotron Radiation Center (Grenoble, France). Figure 1 shows a schematic of the experimental station. The investigated material is placed in a capillary 1 mm in diameter, in which the temperature and gas pressure are controlled by heater *2* and gas distributing system *3* and *4*. The monochromatic X-ray radiation passes from channel *5* downstream of the Si(111) monochromator. The radiation intensity prior to interacting with the sample is measured by ionization chamber *6*.

Semiconductor detector *7* measures the X-ray fluorescence intensity for each value of the energy coming to the sample. It should be noted that in this work, we obtained for the first time Mn *K*-edge X-ray absorption near edge structure (XANES) spectra of $Mn(BH_4)_2$. In measuring the X-ray absorption spectra, the incident radiation energy was changed continuously in the range of 6500–6700 eV; in recording diffraction patterns, the wavelength of the incident radiation was fixed at 0.51323 Å. The diffraction patterns were recorded immediately before measuring each spectrum using a 2D detector. The resulting 2D diffraction patterns were integrated using the Fit2D software package [11].

Theoretical X-ray absorption spectra were obtained in the one-electron approximation using Fermi's golden rule. The X-ray absorption cross section obeyed this rule, so the dipole matrix element for the transition to the continuous spectral states can be written as

$$\sigma(E) \sim \left|\langle \psi_{1s} | \varepsilon \cdot r | \psi_f \rangle\right|^2 \cdot \delta(E - E_f - E_{1s}),$$

where ψ_{1s} and E_{1s} are the wave function and energy of the core electron; ψ_f and E_f are the wave function and energy of the finite unoccupied states; and ε is the photon polarization. The wave functions of unoccupied electron levels were calculated by the finite difference method [12] in a sphere with a radius of 7 Å around the absorbing atom. Calculations for the XANES spectra using the original FDMnes code based on the Gaussian technique require much time, especially for low-symmetry systems. The calculations center on solving a large system of linear equations. Nonzero elements of the system are concentrated near the main diagonal. We established that 95% of the matrix elements were zero and used diagonalization methods that were more suitable for dispersed matrices. Diagonalization using the UMFPACK nonsymmetrical-pattern multifrontal method [12, 13] or a MUMPS multifrontal parallel solver for dispersed matrices [14, 15] can accelerate calculations by factors of 5–20, depending on the input parameters, parallelization options, and computational power. The latter technique is preferred for parallelization on multicore processors, since it requires less random-access memory.

RESULTS AND DISCUSSION

Our samples were synthesized in a high-energy ball grinder and an argon atmosphere. $NaBH_4$ (purity, 95%; Fluka) and waterless $MnCl_2$ (purity, 99.999%; Sigma Aldrich) were manually mixed in molar ratios of 2 : 1 and 3 : 1 in an agate mortar and then ground in the course of high-energy mechanosynthesis. A steel cylinder with three steel balls 15, 12, and 10 mm in diameter was used. The rate of rotation was set at 600 min^{-1}. The ratio between the ball mass and the ground powder mass was 25 : 1. To avoid heating the system and thus powder agglomeration on the cylinder's surface, grinding was interrupted with breaks lasting 5 min. The interruptions were repeated every 10 min. The reaction equation was

$$2NaBH_4 + MnCl_2 \rightarrow NaCl + Mn(BH_4)_2.$$

Samples for spectral investigations were prepared in an inert argon atmosphere. Each powder sample was carefully poured in a glass capillary 1 mm in diameter with a wall thickness of only 10 μm. A constant hydrogen pressure of 10 bar was maintained in each experiment. Our low-temperature Raman spectra coincided with the spectra recorded on the freshly synthesized material [11].

Figure 2 shows the diffraction pattern of a synthesized sample. The structure of the material was resolved via XRD analysis. The final product contains $Mn(BH_4)_2$ and about 5% of $NaBH_4$.

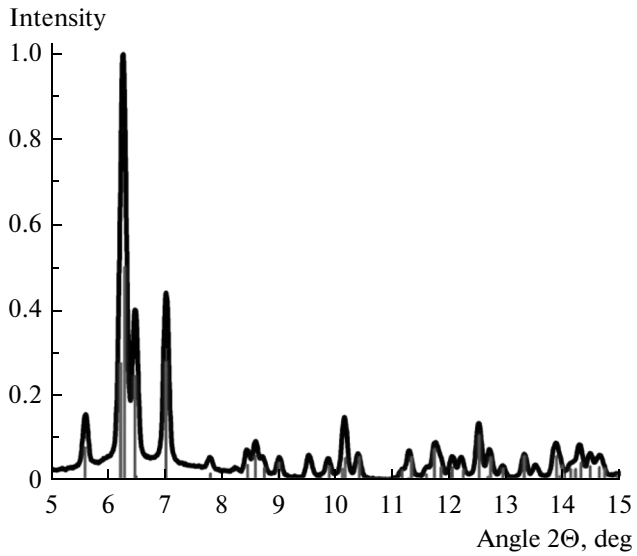

Fig. 2. Experimental diffraction pattern of $Mn(BH_4)_2$ powder (solid curve) and calculated peak positions and intensities for the structure from the crystallographic database.

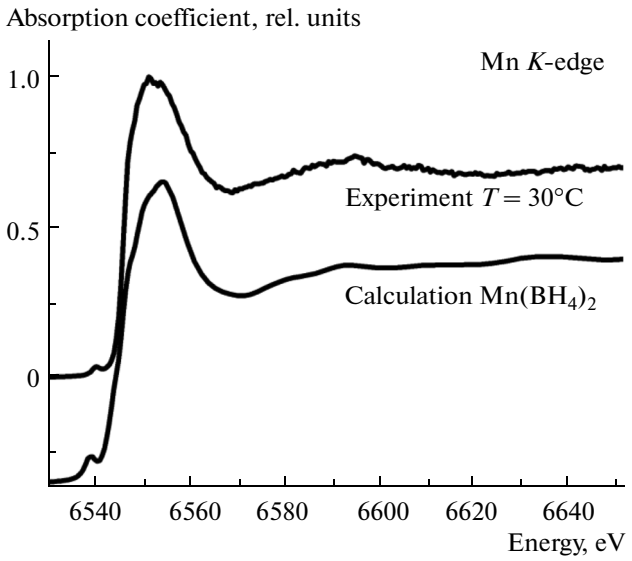

Fig. 3. Experimental Mn *K*-edge XANES spectrum of $Mn(BH_4)_2$ at room temperature and the calculated spectrum of the structure from the crystallographic database.

Since the Mn *K*-edge XANES spectra were recorded in the fluorescence mode, self-absorption effects are clearly visible. The experimental spectra were therefore corrected using the Ifeffit Athena software package [16]. Figure 3 shows the experimental absorption spectrum of manganese borohydride and the theoretical spectrum calculated for the structure obtained by XRD in [7]. It can be seen that the theoretical and experimental spectra are in good agreement, allowing us to use this technique to analyze the phases in a sample after decomposition upon heating.

Thermogravimetric analysis showed that the phase transition was accompanied by a stepwise change in sample mass. The gas mass spectroscopy data indicate the desorption of hydrogen as the main gas product of the reaction with maximum intensity in the temperature range of 130–150°C. In addition, desorption was accompanied by a negligible release of diborane B_2H_6. Although analysis of the partial gas pressure diagrams enables us to determine the qualitative and quantitative composition of the gas reaction products precisely and approximately, determining the composition of solid reaction products is in our case complicated by the amorphization of the material, which broadens the diffraction peaks.

The aim of this investigation was to determine the qualitative composition of the products of decomposition induced by sample heating by analyzing the immediate environment of the Mn atom in the manganese borohydride $Mn(BH_4)_2$ lattice.

Upon heating, the sample changed color from light yellow to black. The spectral variations above 110°C were irreversible (after reaching 200°C, the temperature was reduced to 30°C and the spectra were recorded repeatedly). Above 110°C, it was impossible to detect Raman spectra because of the strong radiation absorption in the sample.

Figure 4 shows XRD patterns at different heating temperatures. The sharpest high-intensity peaks of the $Mn(BH_4)_2$ crystal phase disappeared at $t = 130$°C. According to the data from thermogravimetric and partial gas pressure analysis, the intensity of hydrogen desorption was maximal in the same temperature range. Upon heating, the initial material thus underwent a phase transition accompanied by amorphiza-

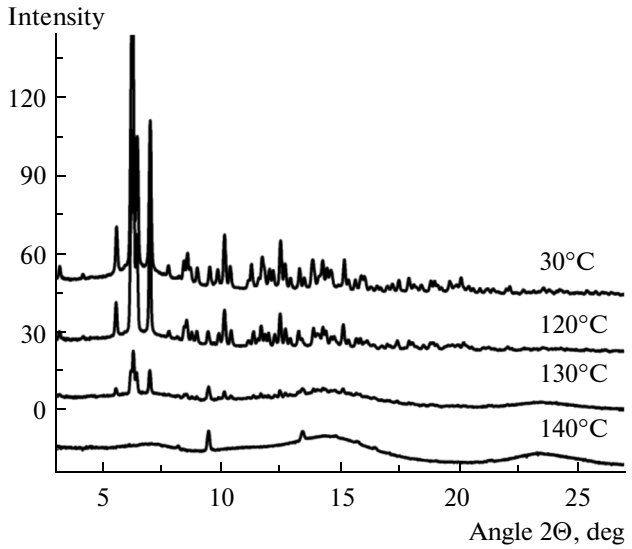

Fig. 4. Experimental XRD spectra obtained in vacuum at different sample temperatures.

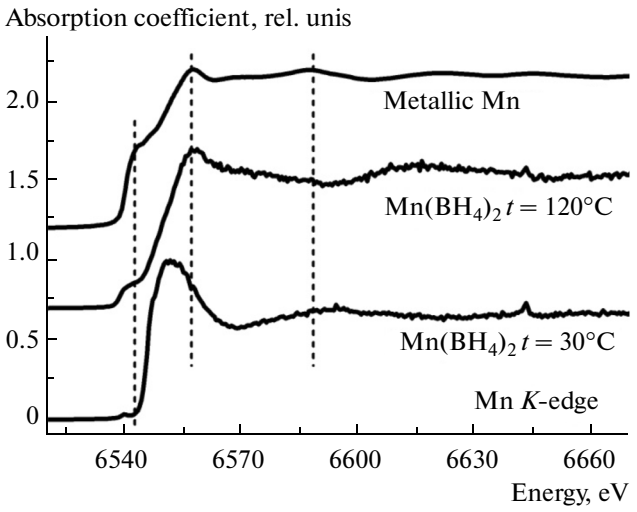

Fig. 5. Experimental Mn *K*-edge XANES spectra of $Mn(BH_4)_2$ and metallic manganese phase Mn_{met}. Manganese borohydride $Mn(BH_4)_2$ under the initial conditions (lower curve) and after heating (middle curve), and metallic manganese phase Mn_{met} under normal conditions (upper curve).

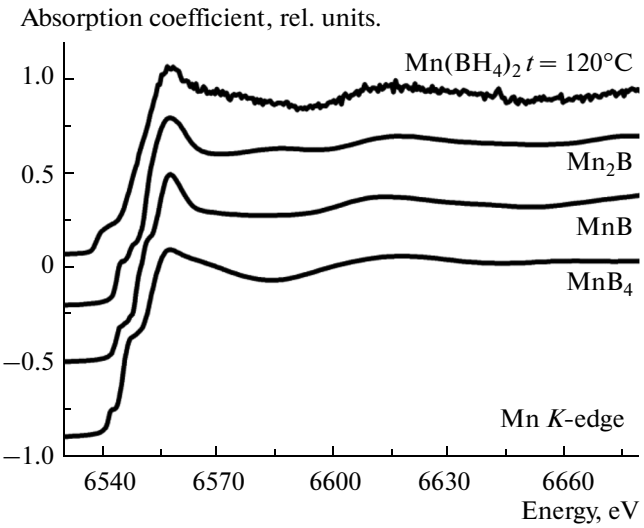

Fig. 6. Experimental Mn *K*-edge XANES spectra of $Mn(BH_4)_2$ after heating and the theoretically calculated spectra of manganese borides.

tion of the sample and hydrogen desorption. The sharp low-intensity peaks in the XRD spectra at $t = 130$°C and $t = 140$°C and angles of 6.5°, 7°, and 9.5° can be explained by the negligible (~5 %) amount of sodium borohydride $Na(BH_4)_2$ that went unreacted during mechanosynthesis.

Figure 5 shows experimental Mn *K*-edge XANES spectra of manganese borohydride $Mn(BH_4)_2$ before heating (lower curve) and after heating at 120°C (middle curve), and those of metallic manganese Mn_{met} (upper curve). In the manganese borohydride spectra, we can clearly see the variations in the energy position of the main maximum and second absorption peak upon sample heating. The Natoli rule [20] was used to establish the correlation between the variation in the energy localization of the spectral features and the change in the interatomic distances in the first coordination sphere of the absorbing atom. According to the Natoli rule, the ratio between the squared interatomic distances in the first coordination sphere of two compounds with similar symmetry is inversely proportional to the corresponding peaks in X-ray absorption spectra. Having measured the distance between the main maximum and the next one in the $Mn(BH_4)_2$ spectra at temperatures of 30 and 120°C in Fig. 5, we may thus conclude that the Mn–B distances in the first coordination sphere of manganese shrank. The averaged estimated reduction in the Mn–B distances upon sample heating was 0.39 Å, relative to the initial value of 2.43 Å.

In [5, 10, 17], where possible paths of $Mn(BH_4)_2$ decomposition were simulated, the metallic manganese phase and diborane B_2H_6 were mentioned among the reaction products, along with boron B and molecular hydrogen H_2. Diborane is a highly volatile and chemically active element. However, it was reported that the intensity of diborane release was lower than that of hydrogen desorption by a factor of 600 [5].

$$Mn(BH_4)_2 \rightarrow Mn + 2B + 4H_2, \quad (1a)$$

$$Mn(BH_4)_2 \rightarrow Mn + B + H_2 + B_2H_6, \quad (1b)$$

$$Mn(BH_4)_2 \rightarrow MnH_2 + 2B + 3H_2, \quad (1c)$$

$$Mn(BH_4)_2 \rightarrow MnB_2 + 4H_2, \quad (1d)$$

$$Mn(BH_4)_2 \rightarrow MnH_2 + B_2H_6, \quad (1e)$$

$$Mn(BH_4)_2 \rightarrow Mn + B_2H_6 + H_2. \quad (1f)$$

The possible paths of decomposition were obtained through calculations using the density functional theory (DFT). In [18], the first reaction was considered to be the one most likely. According to the results from our analysis of the Mn *K*-edge XANES spectra, however, we may conclude that the spectrum of metallic manganese unsatisfactorily describes the experiment with $Mn(BH_4)_2$ after heating. We suggest the presence of other manganese-bearing compounds as the final products of the decomposition reaction. Since there is a lack of literature data, we theoretically calculated the Mn *K*-edge XANES spectra of different manganese borides. The structures of these compounds are available in the ICSD crystallographic database (nos. 42529, 44446, 614742, 44445, and 653726). Analysis of the obtained curves showed that the experimental curve for manganese borohydride after heating was described best by manganese borides Mn_2B, MnB, and MnB_4. The absorption spectra of these compounds are presented in Fig. 6. The spectra of MnB_2 and Mn_3B_4 are inconsistent with the experiment, so we may exclude the possibility of these borides forming.

To describe satisfactorily the experimental spectrum of $Mn(BH_4)_2$, we investigated superpositions of the spectra of the metallic Mn phase and the abovementioned manganese borides. The weight coefficients were fit using the Fitit software package [19] with respect to the self-consistent energy localization of the absorption edge. The fitting of all three borides Mn_2B, MnB, and MnB_4 in combination with metallic manganese Mn_{met} yielded identical residual coefficients, i.e., the parameter characterized by the integral of the absolute value of the difference between the compared spectra in a specified energy range. Hence, the formation of one of the borides Mn_2B, MnB, and MnB_4 as a reaction product in combination with the metallic phase Mn_{met} appears probable. In addition, the results from the XANES spectra fitting clearly show that the maximum estimated concentration of the manganese metallic phase is no more than 35%.

CONCLUSIONS

Families of XRD patterns and Mn *K*-edge XANES spectra were experimentally obtained at different sample temperatures. In the same temperature range of 120 to 140°C, both the XRD and Mn *K*-edge XANES spectra changed dramatically. The considerable broadening of the peaks in the diffraction patterns along with the thermogravimetric analysis data show that a phase transition occured in the abovementioned temperature range and was accompanied by profuse hydrogen desorption, leading to the degradation of the initial material and, as a result, irreversibility of the reaction. Theoretical simulations of the Mn *K*-edge XANES spectra of different manganese borides and subsequent fitting with regard to the formation of the metallic manganese phase show that the most likely intermediate products of decomposition are metal manganese and amorphous borides Mn_2B, MnB, and MnB_4. The estimated metallic manganese concentration was no more than 35%.

ACKNOWLEDGMENTS

We would like to thank Yaroslav Filinchuk for providing our samples and commenting on the experimental technique.

This work was supported by RF Presidential Grant MK-3206.2014.2 for the Support of Young Scientists, and by RF Government Grant 14.Y26.31.0001 for the State Support of Research under the Guidance of Leading Scientists.

REFERENCES

1. Orimo, S.I., Nakamori, Y., Eliseo, J.R., Zuttel, A., and Jensen, C.M., *Chem. Rev.*, 2007, vol. 107, p. 4111.
2. Zuttel, A., Rentsch, S., Fischer, P., Wenger, P., Sudan, P., Mauron, P., and Emmenegger, C., *J. Alloys Compounds*, 2003, vol. 356, p. 515.
3. Zuttel, A., Wenger, P., Rentsch, S., Sudan, P., Mauron, P., and Emmenegger, C., *J. Power Sources*, 2003, vol. 118, p. 1.
4. Kou, H., Sang, G., Huang, Z., Luo, W., Chen, L., Xiao, X., Hu, C., and Zhou, Y., *Int. J. Hydrogen Energy,* 2014, vol. 39, p. 7050.
5. Varin, R.A., Zbroniec, L., Polanski, M., Filinchuk, Y., and Cerny, R., *Int. J. Hydrogen Energy*, 2012, vol. 37, p. 16056.
6. Liu, R.X., Reed, D., and Book, D., *J. Alloys Compounds*, 2012, vol. 32, p. 515.
7. Černý, R., Penin, N., Hagemann, H., and Filinchuk, Y., *J. Phys. Chem. C*, 2009, vol. 113, p. 9003.
8. Filinchuk, Y., Richter, B., Jensen, T.R., Dmitriev, V., Chernyshov, D., and Hagemann, H., *Angew. Chem. Int. Ed.*, 2011, vol. 50, p. 11162.
9. Cerny, N.P.R., Hagemann, H., and Filinchuk, Y., *J. Phys. Chem. C,* 2009, vol. 113, p. 9003.
10. Liu, R., Reed, D., and Book, D., *J. Alloys Compounds*, 2012, vol. 32, p. 515.
11. Hammersley, A.P., Svensson, S.O., Hanfland, M., Fitch, A.N., and Hausermann, D., *High Pressure Res.*, 1996, vol. 14, p. 235.
12. Davis, T.A., *ACM Trans., Math. Softwear*, 2004, vol. 30, p. 196.
13. Davis, T.A. and Duff, I.S., *ACM Trans. Math. Softwear*, 1999, vol. 25, p. 1.
14. Amestoy, P.R., Guermouche, A., L'Excellent, J.-Y., and Pralet, S., *Parallel Comput.*, 2006, vol. 32, p. 136.
15. Amestoy, P., Duff, I., L'Excellent, J., and Koster, J., *SIAM J. Matrix Anal. Appl.*, 2001, vol. 23, p. 15.
16. Shaltout, A.A., Gomma, M.M., and Ali-Bik, M.W., *X-Ray Spectrometry,* 2012, vol. 41, p. 355.
17. Soloveichik, G.L., *Mater. Matters*, 2007, vol. 2.2, p. 11.
18. Choudhury, P., Bhethanabotla, V.R., and Stefanakos, E., *J. Phys. Chem. C,* 2009, vol. 113, p. 13416.
19. Smolentsev, G., Soldatov, A.V., and Feiters, M.C., *Phys. Rev. B*, 2007, vol. 75, p. 144106.
20. Bianconi, A, Dell Ariccia, M., Gargano, A., and Natoli, C.R., in *Bond Length Determination Using XANES. EXAFS and Near Edge Structure*, Bianconi, A., Incoccia, A., and Stipcich, S., Eds., Berlin: Springer, 1987, pp. 57–61.

Translated by E.V. Bondareva